AIAA AVIATION Forum
August 2-6, 2021, VIRTUAL EVENT
AIAA AVIATION 2021 FORUM

10.2514/6.2021-2937

Optimal Pitching in a Transverse Gust Encounter Using a Modified Goman-Khrabrov Model

Xianzhang Xu* and Francis D. Lagor†
University at Buffalo, The State University of New York, Buffalo NY 14260

This paper presents a framework for calculating an optimal pitch maneuver to regulate lift in a transverse gust encounter using a modified Goman-Khrabrov model. A modified Goman-Khrabrov model that uses effective angle of attack has previously been shown to provide a useful low-order, dynamic model of a transverse gust encounter. The effective angle of attack incorporates the effects of kinematic motions and a prescribed flow. The proposed framework poses the lift regulation problem as an optimal control problem that integrates a quadratic cost for lift deviations over a fixed time interval, subject to the dynamics of the modified Goman-Khrabrov model and terminal constraints on pitch angle and pitch rate. A gradient-based optimization algorithm solves for an optimal (open-loop) control signal for pitch acceleration. Simulation results show how the optimal control profile varies with gust strength, gust width, and pitch-axis location. For a given gust, the optimal control derived using the modified Goman-Khrabrov model is compared to proportional output-feedback control of lift. Simulation results show that the output-feedback control signal converges to the optimal control signal, in the absence of measurement noise, as the feedback control gain increases.

I. Nomenclature

Roman Letters

a	=	pitch axis location in semi-chords
b	=	semi-chord length, $c/2$
c	=	chord length
C_L	=	lift coefficient
$C_{L,\text{ref}}$	=	reference value for lift coefficient
$\mathbf{f}(\cdot)$	=	dynamic constraints function
GR	=	gust ratio, $V_{\max}/\overline{V}$
H	=	Hamiltonian in optimal control theory
$\dot{h}$	=	plunge rate
$I_{\psi\psi}, I_{\psi \mathrm{J}}, I_{\mathrm{J}\psi}, I_{\mathrm{JJ}}$	=	integral terms in optimal control algorithm
$J(\cdot)$	=	performance measure for optimal control
$\tilde{J}(\cdot)$	=	performance measure augmented with terminal constraints
K	=	proportional feedback control gain
L	=	Lagrangian function in optimal control theory
$m_1(\cdot), m_2(\cdot)$	=	functions defining bounding curves in the C_L versus angle of attack plane
p	=	number of specified states at the terminal time of optimal control problem
q	=	internal variable in the Goman-Khrabrov lift model
$q_0(\cdot)$	=	empirical function in the Goman-Khrabrov lift model
q_{ref}	=	q value corresponding to $C_{L,\text{ref}}$
$\mathbf{R}(\cdot)$	=	influence co-states for terminal constraint sensitivity in optimal control algorithm
$\dot{s}$	=	surge rate
t^*	=	convective time, Ut/c
t_0, t_f	=	start time and terminal times of the optimal control problem
$u(\cdot)$	=	control input signal
$u_0(\cdot)$	=	initial guess of control input signal in optimal control algorithm
(u', v')	=	components of flow-relative velocity

*Graduate Student, Department of Mechanical and Aerospace Engineering, AIAA Student Member
†Assistant Professor, Department of Mechanical and Aerospace Engineering, AIAA Senior Member

(u_x, u_z)	=	external flow components in the inertial reference frame
$\overline{V}$	=	constant, characteristic flow speed
$V_{\max}$	=	maximum velocity of gust flow model
V_∞	=	speed of freestream flow
W	=	gust width
$\mathbf{x}$	=	state vector
$\mathbf{x}_{\text{ref}}$	=	reference state vector
(x_C, z_C)	=	coordinates of pitching location in the body frame of the wing
y	=	output of the state-space model

Greek Letters

$\alpha, \dot{\alpha}$	=	angle of attack, angle-of-attack rate
α_0	=	angle-of-attack offset of the fully separated linear fit
$\alpha_{\text{eff}}, \dot{\alpha}_{\text{eff}}$	=	effective angle of attack, effective angle-of-attack rate
θ_0	=	angular coordinate of evaluation location on mean camber line
$\theta_g, \dot{\theta}_g, \ddot{\theta}_g$	=	geometric angle of attack, pitch rate, pitch acceleration
$\theta_{g,\text{ref}}, \dot{\theta}_{g,\text{ref}}$	=	reference values for geometric angle of attack and pitch rate
$\boldsymbol{\lambda}$	=	co-state vector to incorporate the dynamic constraint
$\boldsymbol{\nu}$	=	co-state vector to incorporate the terminal constraint
Ξ	=	positive-definite weight matrix in optimal control algorithm
τ_1, τ_2	=	time constants in the Goman-Khrabrov lift model
$\boldsymbol{\psi}(\cdot)$	=	terminal constraint

II. Introduction

Wind gusts and other unsteady flow fields can create significant aerodynamic disturbances for small aircraft such as unmanned air vehicles (UAVs) and micro air vehicles (MAVs), which are vulnerable to large-amplitude gusts due to their relatively small size and low speed [1]. As a result, modeling and control of airloads in unsteady flow fields at low Reynolds numbers is an active area of research [2–4]. Previous research works have developed controllers based on linearized gust models and flight dynamics that consider the gust as an unsteady disturbance input [4, 5]. Aerodynamic response is complex in large-amplitude gust encounter, so a model-based control design that uses an unsteady nonlinear aerodynamic model may provide a better solution for lift regulation [6]. Additionally, control that makes use of a nonlinear model may lead to valuable insights of mechanisms for flow interaction.

Large amplitude gust encounters can lead to massive flow separation (e.g. see Biler et al. [7]), but thin-airfoil models from classical theories have an attached-flow assumption. Recent efforts [7–9] to model transverse gust encounters have examined classical theories to determine the extent of their applicability for large-amplitude gust encounters. Quasi-steady thin-airfoil theory can model slowly varying airfoil behaviors in pitch, plunge, and surge [10]. Transverse gust effects can be expressed in effective angle of attack as an external flow contribution [6, 11]. Classical unsteady thin-airfoil theory developed by Wagner, Theodorsen, Küssner, and von Kármán [12–15] include acceleration terms and wake effects. Classical models provide some predictive power, but nonlinearities are important to capture realistic effects associated with flow separation and re-attachment for a rapidly maneuvering wing in a transverse gust encounter.

Goman and Khrabrov [16] developed a low-order, empirical modeling approach for unsteady aerodynamic forces and moments without an attached-flow assumption [17, 18]. An empirical GK model for lift consists of an internal variable that governs the degree of flow separation, an empirical function for the steady-state values of the internal variable for varying angles of attack, and first-order dynamics that describe deviation from and return to steady state. With two time constants and an empirical steady-state function, GK models are capable of fitting a variety of aerodynamic force behaviors. In addition, the low-order form of the dynamics enables rapid simulation, which is an important consideration in the optimal control framework presented in this paper. Due to the practicality of GK models, several studies [18–20] have used these models to design controllers. For example, Williams and King [20] developed a closed-loop controller based on a modified GK model that can alleviate gust loading during periodic pitching through the use of jet actuators.

Several researchers have modified the original GK model. For example, Sedky et al. [6] modified the GK model to incorporate effective angle of attack, which combines kinematic maneuvering and gust effects. The modified GK model was used in an observer-based feedback controller for a pitching airfoil to reduce the transient lift response during a transverse gust encounter. Experiments in [6] show that the modified GK model can represent a transverse gust

encounter. Narsipur et al. [21] similarly modified the GK model by incorporating the Leading Edge Suction Parameter (LESP). LESP can be used to modulate the shedding of vorticity at the leading edge in a Discrete-Vortex Model (DVM). LESP relates to effective angle of attack through the Fourier coefficients of the airfoil's bound circulation; LESP is the zeroth coefficient [22], and effective angle of attack includes the zeroth and first coefficients [11].

In addition to seeking accurate models for gust encounters that may be useful for control, researchers have examined the mechanisms by which control actuation influences lift during a gust encounter. Sedky et al. [8] deconstructed the force contributions to lift that occurred using proportional feedback control interacting with a DVM of a gust encounter. In experiments, Andreu-Angulo and Babinsky [23] examined different pitch profiles for a flat plate encounter a top-hat gust and described the resulting force contributions from gust vorticity, wing motion, and shed vorticity. These works seek to find pitch maneuvers that can regulate the lift during a gust encounter. The use of simulations [7, 8] and experiments [9] for investigations of the origins of force contributions are useful for understanding the flow physics of the encounter, but these approaches are not readily amenable to optimization of the maneuver.

The question of whether an optimal pitching maneuver exists naturally arises. Obtaining an optimal pitch maneuver is important for the analysis of flow mechanisms exploited by the maneuver. Such a maneuver could also be useful in the design of a trajectory tracking controller or a controller that rejects disturbances about an optimal trajectory. Additionally, an optimal maneuver is an important point of comparison for assessing other control designs. Section V.C compares proportional output-feedback control solutions to an optimal control signal for a gust encounter represented by a modified GK model. Andreu-Angulo and Babinsky [24] proposed an analytical model based on theories of Wagner and Küssner to calculate an ideal pitch profile for maintaining zero lift during an encounter with a top-hat gust. Their model contributes to understanding how classical unsteady aerodynamic theories apply to gust encounters. Andreu-Angulo et al. [9] show that linear models can perform well for low gust ratios (GR ≤ 0.5) and that they may work well for increasing GR, depending on the gust shape. For gust encounters that deviate from the linear unsteady theory, an empirical Goman-Khrabrov model is an available modeling tool. This work also utilizes a modified GK model based on Sedky et al. [6], because it is computationally cheaper than Computational Fluid Dynamics (CFD) or DVM simulations.

This paper seeks an optimal maneuver that minimizes the lift response caused by a transverse gust encounter represented by a modified GK model. This paper also studies an optimal pitch maneuver's variation with changes in gust strength, width, and pitch-axis location. This paper contributes an optimal control framework for minimizing the lift response during a wing-gust encounter and a comparison of the optimal maneuver to proportional output-feedback control. The results show that an optimal control profile can be generated by using proportional output feedback. These contributions are important because the framework can generate optimal maneuvers for a various wing and gust profiles, provided the wing-gust interaction can be reasonably represented by a modified GK model. Furthermore, the numerical results that compare to proportional output-feedback control suggest that an optimal maneuver can easily be found using proportional output-feedback control without performing the optimal-control calculations when a modified GK model is used.

The outline of this paper is as follows. Section III presents background information on effective angle of attack and the modified GK model of a gust encounter. Section IV formulates the optimal-control problem for a gust encounter. Section V presents simulation results for various gusts, and compares to proportional output-feedback control. Section VI concludes the paper and discusses ongoing work.

III. Gust Encounter Modeling

This section presents the use of a GK model to capture the unsteady aerodynamic response of a wing in a gust encounter. Using effective angle of attack in the GK model modifies it to incorporate the influence of a prescribed gust flow field. This section also puts the model in state-space form for the optimal control framework in Section IV.

A. Goman-Khrabrov Lift Model

Goman and Khrabrov [16] developed a low-order model for lift force during unsteady pitching motion through high angles of attack where flow separation is present. The GK model captures the dynamic flow state with an internal variable q that describes the extent of flow attachment [17]. Let α be the geometric angle of attack, and let C_L be the dimensionless lift coefficient. The GK model is [25]

$$\tau_1 \dot{q} + q = q_0 \left(\alpha - \tau_2 \dot{\alpha}\right) \tag{1}$$

$$C_L = m_1(\alpha)\, q + m_2(\alpha)\,(1 - q) \tag{2}$$

where $q_0(\cdot)$ is an empirical function obtained from steady conditions, and $m_1(\cdot)$ and $m_2(\cdot)$ are empirical functions of α that bound the lift curve and its variations in time in the C_L vs. α plane. When the angle of attack increases from low to high, the value of q varies from approximately 1, representing fully attached, to 0, representing fully separated. The empirical function $q_0(\cdot)$ is a scalar curve that varies from approximately 1 to 0 and provides steady-state values for the q dynamics for various angles of attack. Time constants τ_1 and τ_2 indicate the time for separated flow to reach steady state and a time constant for rate of change of angle of attack effects, respectively. After the original work of Goman and Khrabrov, some researchers [18, 19, 25] have assigned physical meaning to the two bounding curves in Eq. (2) as

$$\begin{aligned} m_1(\alpha) &= \left.\frac{\partial C_L}{\partial \alpha}\right|_{\text{attached}} \alpha, \\ m_2(\alpha) &= \left.\frac{\partial C_L}{\partial \alpha}\right|_{\text{sep}} (\alpha - \alpha_0) \end{aligned} \tag{3}$$

where $m_1(\alpha)$ fits the steady C_L versus α curve in the region where the flow is fully attached, and $m_2(\alpha)$ fits the curve in the fully separated region. Occasionally lift curves deviate from an ideal curve shape (e.g., see [6]), in which case m_1 and m_2 can be chosen to enclose a convex region of the plane that contains the lift data, as shown in Fig. 1(a). In this paper, in order to develop an optimal trajectory using optimal control theory, q_0 is parameterized by a Gaussian function as shown in Fig. 1(b). A Gaussian fit is justified by the objective of this work to investigate general trends in control maneuvers during gust encounters; direct use of a noisy q_0 curve would complicate the analysis with a wing-specific characteristics from the experimental data. This paper uses empirical wing data from [26] for the GK model, which is relevant to current research [7, 8] on gust encounters for wings encountering strong gusts with gust widths on the order of the wing chord.

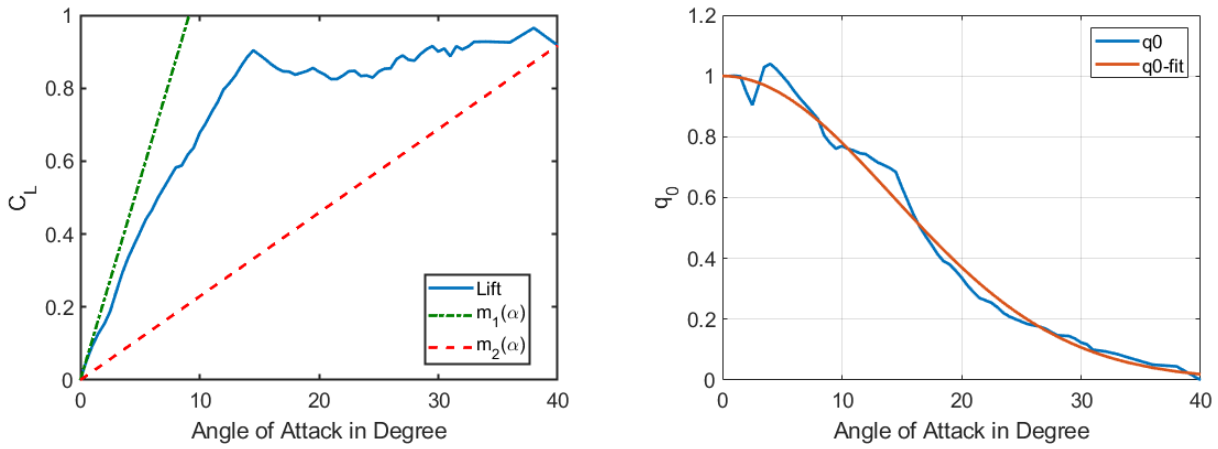

(a) **(b)**

Fig. 1 a) Steady C_L vs. α curve for a NACA 0012 finite wing with bounding curves $m_1(\alpha)$ and $m_2(\alpha)$. b) Empirical function q_0 vs. α and a Gaussian curve fit. Data in plots comes from [26].

B. Effective Angle of Attack

Effective angle of attack is a composite quantity that integrates effects from an external flow field with effects from kinematic motions such as pitching, plunging, and surging. For a thin-airfoil of semi-chord b pitching and plunging in a freestream with speed V_∞, classical quasi-steady effective angle of attack is [10]

$$\alpha_{\text{eff}} = \alpha + \frac{\dot{h}}{V_\infty} + b\left(\frac{1}{2} - a\right)\frac{\dot{\alpha}}{V_\infty}, \tag{4}$$

where $\dot{h}$ is the plunge rate, $\dot{\alpha}$ is the pitch rate, and a locates the pitch axis along the chord. In [11], the authors present an effective angle of attack expression

$$\alpha_{\text{eff}} = -\frac{1}{\pi}\int_0^{\pi} \frac{w' - u'\frac{dz}{dx}}{\overline{V}\sqrt{1+\left(\frac{dz}{dx}\right)^2}}\left(\cos\theta_0 - 1\right) d\theta_0, \tag{5}$$

that incorporates the external flow effects by integrating the local flow velocity along the chord, where $\overline{V}$ is a characteristic flow speed, and θ_0 is a coordinate that parameterizes the airfoil chord from $\theta_0 = 0$ at the leading edge to $\theta_0 = \pi$ at the trailing edge. This effective angle of attack expression contains the camber line $z\left(\theta_0\right)$ and camber slope dz/dx, so that it is also applicable for cambered airfoils. The relative velocity components at location θ_0 are

$$u'\left(\theta_0\right) = \left(\dot{s} - u_x\right)\cos\theta_g - \left(\dot{h} - u_z\right)\sin\theta_g - \dot{\theta}_g\left(z\left(\theta_0\right) - z_C\right), \tag{6}$$

$$w'\left(\theta_0\right) = \left(\dot{s} - u_x\right)\sin\theta_g + \left(\dot{h} - u_z\right)\cos\theta_g + \dot{\theta}_g\left(\frac{c}{2}\left(1 - \cos\theta_0\right) - x_C\right). \tag{7}$$

The local velocity components $u'\left(\theta_0\right)$ and $w'\left(\theta_0\right)$ include the external flow components u_x and u_z, and surging, pitching, and plunging terms, $\dot{s}$, $\dot{\theta}_g$, and $\dot{h}$, respectively. Here, θ_g is the geometric angle of attack of the airfoil. The notation for the angle of attack α is replaced in this paper by θ_g to highlight that θ_g represents only the orientation angle of the wing; the local angle of the external flow enters from the (u_x, u_z) flow components in α_{eff}. The coordinates of the pitch-axis center in airfoil's body frame are (x_C, z_C). In [11], the authors show that for a maneuvering symmetric airfoil in uniform flow, the expression of effective angle of attack (5) properly encompasses the classical quasi-steady effective angle of attack in (4). In subsequent sections, this paper considers a pitching symmetric airfoil. For this scenario, effective angle of attack simplifies to

$$\alpha_{\text{eff}} = -\frac{1}{\pi}\int_0^{\pi} \frac{\left[\dot{s}\sin\theta_g - u_z\cos\theta_g + \dot{\theta}_g\left(\frac{c}{2}\left(1-\cos\theta_0\right) - x_C\right)\right]\left(\cos\theta_0 - 1\right)}{\overline{V}} d\theta_0. \tag{8}$$

In the modified GK model, the rate of change of effective angle of attack can be derived by differentiating Eq. (8) with respect to time, yielding

$$\dot{\alpha}_{\text{eff}} = -\frac{1}{\pi}\int_0^{\pi} \frac{\dot{s}\dot{\theta}_g\cos\theta_g + u_z\dot{\theta}_g\sin\theta_g - \dot{u}_z\cos\theta_g + \ddot{\theta}_g\left(\frac{c}{2}\left(1-\cos\theta_0\right) - x_c\right)\left(\cos\theta_0 - 1\right)}{\bar{V}} \tag{9}$$

Note the appearance of the pitch acceleration $\ddot{\theta}_g$ which serves as the control variable in Section IV.

C. The Modified GK Model for Gust Encounters

Sedky et al. [6] present a modified GK model that allows for the incorporation of a gust by replacing the geometric angle of attack and the pitch rate in Eqs. (1) and (2) by the effective angle of attack and its rate of change, respectively. Additionally, Sedky et al. [6] include an added-mass term to model added-mass effects due to rapid maneuvers. Using Theodorsen's expression for added mass [12], the modified GK model used in this paper (hereafter, the mGK model) is

$$\begin{aligned} \dot{q} &= \frac{1}{\tau_1}\left(-q + q_0\left(\alpha_{\text{eff}}\left(\theta_g, \dot{\theta}_g\right) - \tau_2\dot{\alpha}_{\text{eff}}\left(\theta_g, \dot{\theta}_g, \ddot{\theta}_g\right)\right)\right) \\ C_L &= m_1\left(\alpha_{\text{eff}}\left(\theta_g, \dot{\theta}_g\right)\right)q + m_2\left(\alpha_{\text{eff}}\left(\theta_g, \dot{\theta}_g\right)\right)(1-q) + \frac{\pi b}{\overline{V}}\left(\dot{\theta}_g - \frac{ab}{\overline{V}}\ddot{\theta}_g\right). \end{aligned} \tag{10}$$

Equation (10) incorporates gust effects through the effective angle of attack. Note that the effective angle of attack is a function of θ_g and $\dot{\theta}_g$ while the time derivative of effective angle of attack is a function of θ_g, $\dot{\theta}_g$, and $\ddot{\theta}_g$. The explicit $\dot{\theta}_g$ and $\ddot{\theta}_g$ terms in the C_L output equation are added-mass terms. Added mass describes the inertial resistance of fluid surrounding the body during acceleration of the body [27]. The added-mass force required to accelerate this inertia can greatly influence the lift for a maneuvering wing. Even though there may be added-mass effects included in a trained GK model, Sedky et al. [6] insert an added-mass term in the C_L output equation to account explicitly for the contribution of the wing's pitching motion to added mass. This choice is justified because Sedky et al. [6] trained their GK model on a non-maneuvering wing encountering a gust.

The optimal control framework in Section IV requires the system's dynamics to be in state-space form. Define the state vector

$$\mathbf{x} = \begin{bmatrix} x_1 \\ x_2 \\ x_3 \end{bmatrix} = \begin{bmatrix} \theta_g \\ \dot{\theta}_g \\ q \end{bmatrix}, \tag{11}$$

and the output,

$$y = C_L\left(\alpha_{\text{eff}}\left(\theta_g, \dot{\theta}_g\right), q, \ddot{\theta}_g\right),$$

Furthermore, let the pitch acceleration $\ddot{\theta}_g$ be the control input u, such that $\ddot{\theta}_g = u$. By differentiating the state vector and substituting for the state and control variables, the mGK model (10) becomes

$$\begin{bmatrix} \dot{x}_1 \\ \dot{x}_2 \\ \dot{x}_3 \end{bmatrix} = \begin{bmatrix} x_2 \\ u \\ \frac{1}{\tau_1}\left(-x_1 + q_0\left(\alpha_{\text{eff}}\left(x_2, x_3\right) - \tau_2 \dot{\alpha}_{\text{eff}}\left(x_2, x_3, u\right)\right)\right) \end{bmatrix}, \tag{12}$$

$$y = m_1 \alpha_{\text{eff}} x_3 + m_2 \alpha_{\text{eff}}\left(1 - x_3\right) + \frac{\pi b}{\overline{V}}\left(x_2 - \frac{ab}{\overline{V}} u\right).$$

State-space form (12) differs from the form in Sedky et al. [6] because the state variables in [6] are error states relative to a reference flight condition that is useful in the design of their state-feedback controller. The optimal control framework in Section IV of this paper does not require the use of error dynamics. Also, the effective angle of attack α_{eff} is not treated as a state variable since it is a known function of the other states, however, $\alpha_{\text{eff}}(\cdot)$ and $\dot{\alpha}_{\text{eff}}(\cdot)$ are retained in Eq. (12) for notational brevity. The order of the variables in the state vector also differs from [6] because the state-space form (12) is designed for the numerical gradient algorithm in the optimal control framework of Section IV. The algorithm requires variables that are treated as unconstrained at the terminal time to be listed last in the state vector. This paper does not constrain q at the terminal time, so it appears last in the state vector.

To evaluate the ideal velocity from a non-deforming gust (i.e., a gust that influences the wing but is not influenced by the wing) at location θ_0 along the chord, consider the sine-squared gust profile given by [6]

$$u_z(\theta_0, t) = \begin{cases} -V_{\max} \sin^2\left(\frac{\dot{s}t - b(1-\cos\theta_0)}{W}\pi\right) & \text{if} \quad 0 \le \frac{\dot{s}t - b(1-\cos\theta_0)}{W} \le 1, \\ 0 & \text{otherwise,} \end{cases} \tag{13}$$

where $V_{\max}$ is the maximum speed of the gust and W is the gust width. The gust ratio GR is a non-dimensional description of the strength of a sine-squared gust and is given by $\text{GR} = V_{\max}/\overline{V}$. The piece-wise construction of (13) permits the evaluation of gust velocity along the chord with portions of the airfoil outside of the gust region. The piece-wise gust function (13) provides the external flow term needed to evaluate Eqs. (8) and (9). Although the simulations in this paper use a sine-squared gust, the mGK model in (12) and the optimal control framework in Section IV apply to any specified external flow field for a non-deforming gust.

Figure 2 shows simulation results of the mGK model (12) for an airfoil passing through gusts with a fixed gust width but various gust ratios. The airfoil does not maneuver and holds a constant geometric angle of attack, $\theta_g = 5°$. The reference states are: $x_1 = 5°, x_2 = 0$, and $x_3 = 0.94$, and the reference output is $C_{\text{L,ref}} = 0.39$. The time constants τ_1 and τ_2 are referenced from [6], with $\tau_1 = 0.382s$ and $\tau_2 = 0.107s$. The gust width is $3c$, and the gust ratio varies from 0.25 to 1.25. The gray area denotes the gust region, and the vertical dashed line indicates when the wing's trailing edge exits the gust. The results are shown in non-dimensional convective time, $t^* = Ut/c$.

Figure 2(a) captures general features commonly seen in gust encounter experiments [6–8], including a large lift overshoot and a lift undershoot that occurs after the wing exits the gust. Figure 2 shows that C_L, q, and α_{eff} curves vary proportionally with gust ratio, without significant changes in shape. Figure 2(b) shows one notable feature that the q curves group closely for gust ratios greater than 0.75, resulting in similar C_L characteristics for $t^* \ge 3$. The next section introduces a control framework for optimally mitigating the lift overshoot and undershoot in Fig 2(a) for gust ratios in the range $\text{GR} = 0.25 - 1.25$.

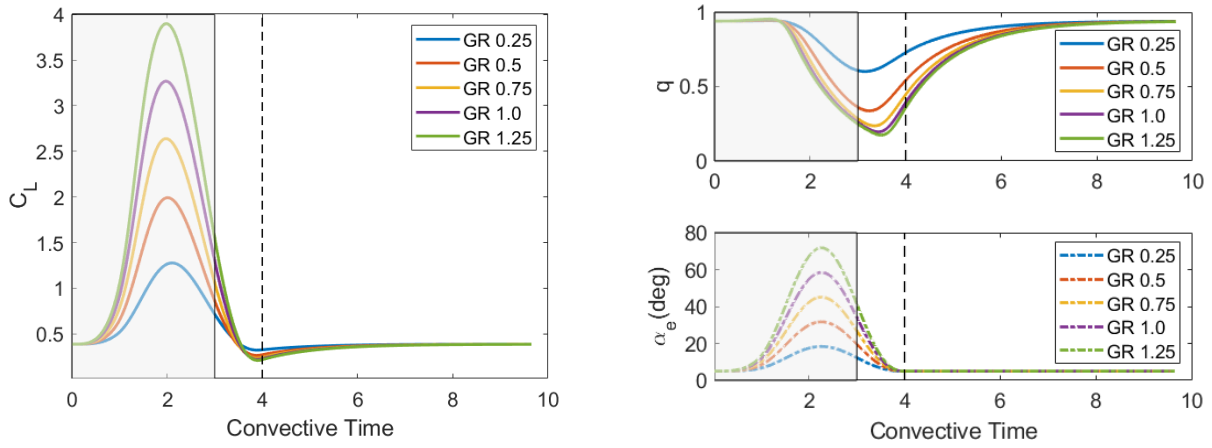

(a) **(b)**

Fig. 2 Simulations of an airfoil in a transverse gust encounter. (a) The lift response, (b) GK model state q, and α_{eff}.

IV. Optimal Control in a Transverse Gust Encounter

This section seeks to regulate lift in a transverse gust encounter by maintaining the lift coefficient as close as possible to a constant value in time by reducing lift transients during the encounter. The objective of regulating lift during and after a gust encounter is equivalent to an optimal trajectory design problem in which the wing's method of actuation serves as the control input. This section presents the framework for optimal control in the design of a trajectory during a fixed time interval with terminal constraints. Subsequently, this section specializes this problem for a gust encounter represented by an mGK model.

A. Optimal Trajectory Problem Statement with Some Terminal States Specified

Consider a fixed time interval $[t_0, t_f]$, and let $x_j\left(t_f\right) = x_{\text{f},j}$ for $j = 1, \ldots, p$ be state components specified at the terminal time. The optimal trajectory problem seeks an open-loop optimal control signal u that solves

$$\begin{aligned} \min_{u} \quad & J(u) = \int_{t_0}^{t_f} L\left(\mathbf{x}, u, t\right) dt \\ \text{subject to} \quad & \dot{\mathbf{x}} = \mathbf{f}\left(\mathbf{x}, u, t\right) \quad \text{with} \quad \mathbf{x}\left(t_0\right) = \mathbf{x_0} \\ & 0 = \boldsymbol{\psi}\left(\mathbf{x}\left(t_f\right)\right) \end{aligned} \tag{14}$$

where the functional $L\left(\cdot\right)$ is the integrand of the performance measure J, $\mathbf{f}\left(\cdot\right)$ represents the system dynamics, and $\boldsymbol{\psi}\left(\cdot\right)$ is a vector of terminal constraints for p specified states, such that $\psi_j = x_j\left(t_f\right) - x_{\text{f},j}$ for $j = 1, \ldots, p$. Equation (14) represents an optimal control problem subject to the systems dynamics as a constraint and some state variables constrained at the terminal time.

The performance measure J in the optimal control problem (14) can be re-written by adjoining the terminal state constraints using a Lagrange multiplier vector $\boldsymbol{\nu}$ and adjoining the system dynamics using a vector of time-varying Lagrange multipliers known as co-states $\boldsymbol{\lambda}$. The augmented performance measure is

$$\tilde{J} = \boldsymbol{\nu}^T \boldsymbol{\psi}\left(\mathbf{x}\left(t_f\right)\right) + \int_{t_0}^{t_f} L\left(\mathbf{x}, u, t\right) + \boldsymbol{\lambda}^T\left(\mathbf{f} - \dot{\mathbf{x}}\right) dt. \tag{15}$$

Note that if the terminal and dynamic constraints are satisfied, $\tilde{J}$ equals J. To derive the first-order necessary conditions for stationarity, it is useful to define a Hamiltonian function $H = L + \boldsymbol{\lambda}^T \mathbf{f}$. Using techniques from the Calculus of Variations, the first order necessary conditions are [28]:

$$\dot{\mathbf{x}} = \left(\frac{\partial H}{\partial \boldsymbol{\lambda}}\right)^T, \quad \text{with} \quad \mathbf{x}\left(t_0\right) = \mathbf{x}_0, \tag{16}$$

$$\dot{\boldsymbol{\lambda}} = -\left(\frac{\partial H}{\partial \mathbf{x}}\right)^T, \quad \text{with} \quad \lambda_j\left(t_f\right) = \begin{cases} \nu_j, & j = 1, \ldots, p \\ 0, & j = p+1, \ldots, n \end{cases} \tag{17}$$

$$0 = \frac{\partial H}{\partial u}, \tag{18}$$

$$x_j\left(t_f\right) = x_{\mathrm{f},j}, \quad \text{for} \quad j = 1, \ldots, p. \tag{19}$$

An optimal control u must satisfy conditions (16) – (19), which form a two-point boundary-value problem, with initial states and some terminal states specified.

Bryson and Ho [28] present a gradient-based method to solve for a candidate optimal control signal that satisfies (16) – (19). For an initial guess of control signal u_0, the corresponding state trajectory $\mathbf{x}$ can be determined from (16). The co-state values at the terminal time should satisfy (17), however, the Lagrange multiplier vector $\boldsymbol{\nu}$ is not known *a priori*. The method of Bryson and Ho [28] solves the co-state equation (17) from zero terminal condition $\boldsymbol{\lambda}\left(t_f\right) = 0$ backward in time, which corresponds to a co-state solve in a problem without state components specified at the terminal time. To deal with state constraints at the terminal time, Bryson and Ho [28] perform p influence (or sensitivity) co-state solves backwards in time from terminal conditions in which the jth entry is 1 and all other entries are 0 for $j = 1, \ldots, p$. These influence solves provide co-state trajectories that are useful in determining how the jth component of $\mathbf{x}\left(t_f\right)$ is affected by a change in the control signal. Collecting the influence co-state solves together in the columns of an influence matrix $\mathbf{R}$, these solves can be accomplished simultaneously using the matrix differential equation [28]

$$\dot{\mathbf{R}} = -\left(\frac{\partial \mathbf{f}}{\partial \mathbf{x}}\right)^T \mathbf{R}, \quad \mathbf{R}_{\mathrm{ij}}\left(t_f\right) = \begin{cases} 1, & i = j, \quad i = 1, \ldots, n \\ 0, & i \neq j, \quad j = 1, \ldots, p. \end{cases} \tag{20}$$

using the result of the influence solves, Bryson and Ho [28] define integrals useful in calculating the Lagrange multiplier vector $\boldsymbol{\nu}$. They subsequently update the control guess in the $-\partial H/\partial u$ direction. Alg. I presents the numerical method of Bryson and Ho [28]. The iterative algorithm is designed to improve the control signal, moving it closer to satisfying the necessary conditions and boundary conditions in Eqs. (16) – (19) with each step [28].

Alg. I: Optimal Control Algorithm for Fixed-Time Problems with Partially Specified Terminal State [28]

Input: Initial guess of control signal $\boldsymbol{u}_0$.

1) Solve the state equation numerically from $\boldsymbol{x}(t_0)$ to t_f.
2) Using the state trajectory obtained in step (1), numerically solve the co-state equation (17) backward from $\boldsymbol{\lambda}\left(t_f\right) = 0$, and solve the influence equation in Eq. (20).
3) Calculate the following integrals:

$$\begin{aligned} I_{\psi\psi} &= \int_{t_0}^{t_f} \mathbf{R}^T \frac{\partial \mathbf{f}}{\partial u} \Xi^{-1} \frac{\partial \mathbf{f}}{\partial u}^T \mathbf{R}\, dt \\ I_{\mathrm{J}\psi} = I_{\psi\,\mathrm{J}}^T &= \int_{t_0}^{t_f} \left(\boldsymbol{\lambda}^T \frac{\partial \mathbf{f}}{\partial u} + \frac{\partial L}{\partial u}\right) \Xi^{-1} \frac{\partial \mathbf{f}}{\partial u}^T \mathbf{R}\, dt \\ I_{\mathrm{JJ}} &= \int_{t_0}^{t_f} \left(\boldsymbol{\lambda}^T \frac{\partial \mathbf{f}}{\partial u} + \frac{\partial L}{\partial u}\right) \Xi^{-1} \left(\boldsymbol{\lambda}^T \frac{\partial \mathbf{f}}{\partial u} + \frac{\partial L}{\partial u}\right)^T dt, \end{aligned} \tag{21}$$

   where the weight matrix Ξ is a user-defined, positive-definite matrix that influences the step size of the algorithm.
4) Evaluate the stopping criteria to determine if the current control signal is satisfactory. Stop when $\boldsymbol{\psi}\left(x\left(t_f\right)\right) = 0$ and $I_{\mathrm{JJ}} - I_{\mathrm{J}\psi} {I_{\psi\psi}}^{-1} I_{\psi\mathrm{J}} = 0$, to within desired tolerance.
5) Select a values of ϵ for a desired update in the terminal constraint, $\delta\boldsymbol{\psi} = -\epsilon\boldsymbol{\psi}\left(x\left(t_f\right)\right), 0 < \epsilon \leq 1$, to obtain the Lagrange multiplier vector

$$\boldsymbol{\nu} = -I_{\psi\psi}^{-1}\left(\delta\boldsymbol{\psi} + I_{\psi\mathrm{J}}\right). \tag{22}$$

Update the control signal u according to

$$\delta u\left(t\right) = -\Xi^{-1}\left(\frac{\partial L}{\partial u} + \left(\boldsymbol{\lambda}\left(t\right) + \mathbf{R}\boldsymbol{\nu}\right)^{T}\frac{\partial L}{\partial u}\right)^{T}, \tag{23}$$

and return to step (1).

Output: Candidate optimal control signal u.

B. Optimal Control Problem Using the Modified GK Model

Prior to the gust encounter, the wing flies at a steady reference flight condition

$$\begin{bmatrix} x_1\left(t_0\right) \\ x_2\left(t_0\right) \\ x_3\left(t_0\right) \end{bmatrix} = \begin{bmatrix} \theta_{\mathrm{g,ref}} \\ \dot{\theta}_{\mathrm{g,ref}} \\ q_{\mathrm{ref}} \end{bmatrix} \tag{24}$$

that corresponds to a constant lift coefficient $C_{L,\mathrm{ref}}$ for $\dot{\theta}_{\mathrm{g,ref}} = 0$. Lift regulation seeks to maintain the lift coefficient as close as possible to the constant $C_{L,\mathrm{ref}}$ value throughout time. To implement C_L regulation, this paper uses pitch acceleration $\ddot{\theta}_g$ as the control input, such that $u = \ddot{\theta}_g$.

An appropriate performance measure for penalizing deviations of the output lift coefficient from the reference lift coefficient is

$$J = \frac{1}{2}\int_{t_0}^{t_f}\left(y - C_{L,\mathrm{ref}}\right)^2 dt. \tag{25}$$

Therefore, the integrand of the performance measure is

$$L\left(\mathbf{x}, u, t\right) = \frac{1}{2}\left(m_1\alpha_{\mathrm{eff}}\left(x_1, x_2\right)x_3 + m_2\alpha_{\mathrm{eff}}\left(x_1, x_2\right)\left(1 - x_3\right) + \frac{\pi b}{\overline{V}}\left(x_2 - \frac{ab}{\overline{V}}u\right) - C_{\mathrm{L,ref}}\right)^2. \tag{26}$$

The terminal time t_f is chosen to be five time constants τ_1 after the time that the trailing edge leaves the gust. This choice is based on providing sufficient time for the q variable in the mGK model to reach a steady-state value. Note that in the open-loop cases in Fig. 2(b), this time is sufficient for the q state to recover. At the terminal time, the wing's state should return to the same reference flight condition that it had prior to the gust encounter, as shown in Eq. (24). However, constraining all states at the terminal time greatly reduces the performance of Alg. I for a lift regulation problem, because the algorithm tries to pitch the wing to strictly enforce $q\left(t_f\right) = q_{\mathrm{ref}}$ at the terminal time. The dynamics of the mGK model naturally drive q to q_{ref} after the wing stops maneuvering. Hence, strictly enforcing $q\left(t_f\right) = q_{\mathrm{ref}}$ is not necessary in practice. Requiring that $\theta_g\left(t_f\right) = \theta_{g,\mathrm{ref}}$ and $\dot{\theta}_g\left(t_f\right) = \dot{\theta}_{g,\mathrm{ref}}$ at the terminal time and penalizing deviations of the output from $C_{L,\mathrm{ref}}$ are sufficient to ensure that $q\left(t_f\right)$ is nearly equal to q_{ref} for the terminal time t_f selected in this work. By constraining only two of the three state components at the terminal time, the terminal constraint vector becomes

$$\boldsymbol{\psi}\left(\mathbf{x}_{t_f}\right) = \begin{bmatrix} x_1\left(t_f\right) - \theta_{\mathrm{g,ref}} \\ x_2\left(t_f\right) - \dot{\theta}_{\mathrm{g,ref}} \end{bmatrix}. \tag{27}$$

The mGK model and the selection of the performance measure, time interval, and initial and terminal conditions fully specify the optimal trajectory problem for lift regulation. Remaining details of derivatives necessary to implement Alg. I are available in the Appendix.

V. Optimal Control Simulation Results

A. Optimal Pitch Maneuvers for Various Gust Strengths and Widths

Optimal control calculations were performed with different gust ratios and gust widths to demonstrate the optimal control framework from Section IV. The gust ratios were GR = 0.25, 0.5, 0.75, 1.0, and 1.25. The gust widths were $W = 1c, 3c$, and $5c$. The optimal control solver iterated until the stopping criteria were met within a tolerance of 5×10^{-8}.

Figure 3 shows the lift coefficient of a wing during gust encounters for gust widths $W = 1c, 3c$, and $5c$, with gust ratio GR = 1.25. The gray area is the gust region and the vertical dashed line indicates when the trailing edge of the wing exits the gust. The blue line represents lift coefficient of a non-maneuvering wing, and the black line corresponds to the wing performing an optimal pitch maneuver. The initial guess of control signal was zero for all time. Note that the lift coefficients of the maneuvering wing are nearly the constant value of $C_{L,\text{ref}} = 0.39$ for all time. The optimal control signal successfully mitigates the lift overshoot during the gust and the lift undershoot after the wing exits the gust while maintaining the lift coefficient at nearly the reference value for the entire period. The optimal controller works well for each of the gust widths considered. Figure 3 examines the strongest gust ratio considered in this paper (i.e., GR = 1.25), which is a typical strong gust ratio in current research on the unsteady aerodynamics of gust encounters [7–9]. Lift coefficient plots for all gust ratios considered in this paper similarly show nearly zero deviation from $C_{L,\text{ref}}$, so additional C_L history plots are omitted.

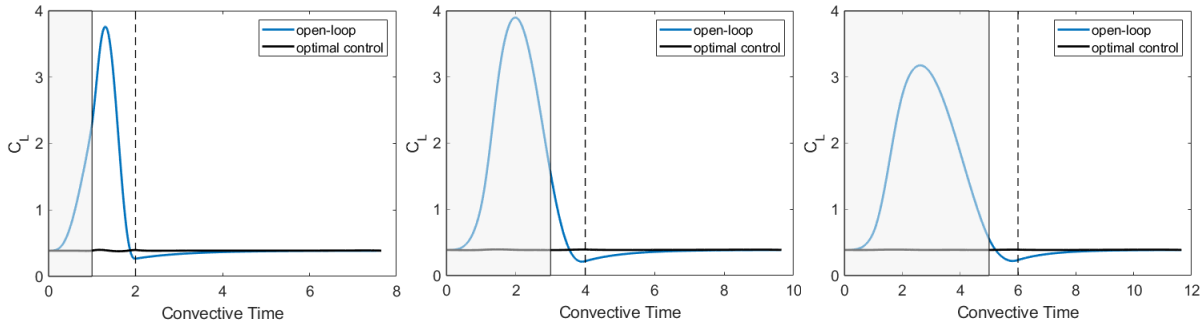

(a) $W = 1c$ **(b)** $W = 3c$ **(c)** $W = 5c$

Fig. 3 Lift coefficient in transverse gust encounters of various widths for a non-maneuvering wing and an optimally maneuvering wing.

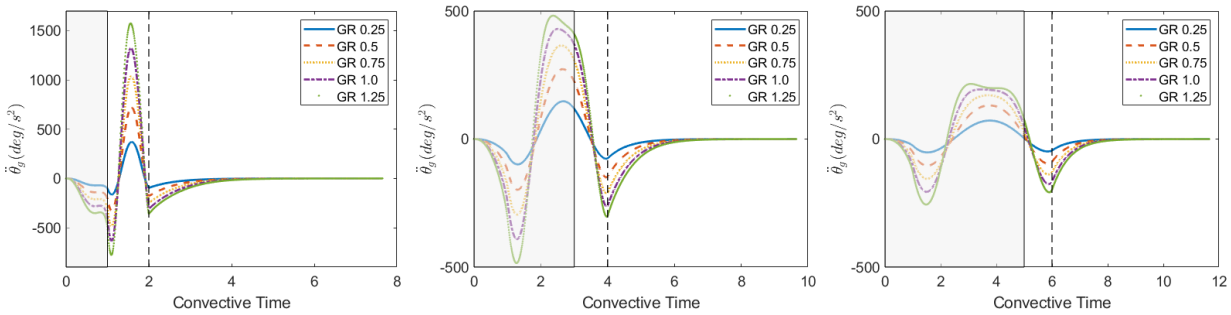

(a) $W = 1c$ **(b)** $W = 3c$ **(c)** $W = 5c$

Fig. 4 Control input $u = \ddot{\theta}_g$ during various gust encounters.

Figure 4 presents the control histories for $\ddot{\theta}_g$ during all gust encounters studied, for gust widths $W = 1c, 3c$, and $5c$, with gust ratios varying from 0.25 to 1.25. For each gust width, the magnitude of the pitch acceleration is generally proportional to the gust ratio, which agrees with the intuition that stronger gusts require greater maneuvering. All of the optimal control profiles display three portions of the curve, corresponding to negative, then positive, then negative pitch acceleration. These signs of pitch acceleration are consistent with a pitch-down, then pitch-up maneuver (i.e., a decreasing ,then increasing pitch angle). All optimal control signals also exhibit a cusp-like feature that occurs at the instant the trailing edge of the wing fully exits the gust. For the narrow $W = 1c$ gust in Fig. 4(a), the pitch acceleration is substantially larger in magnitude than the wider gusts. The wing also finishes the pitch maneuver much sooner due to the reduced time of the gust encounter. Much of the maneuvering in the $W = 1c$ gust occurs as the wing exits the gust region, which may due to the magnitude of the time constant τ_1 relative to the convective time of the gust encounter. Additionally, the effective angle of attack displays a slow increase in magnitude in Fig. 2(b) that could contribute to a delay in response for a maneuvering wing. Other noteworthy differences in the control profiles occur before the wing exits the narrow $W = 1c$ gust. These shape differences may also be attributed to the narrow gust width and the relatively

brief duration of the encounter.

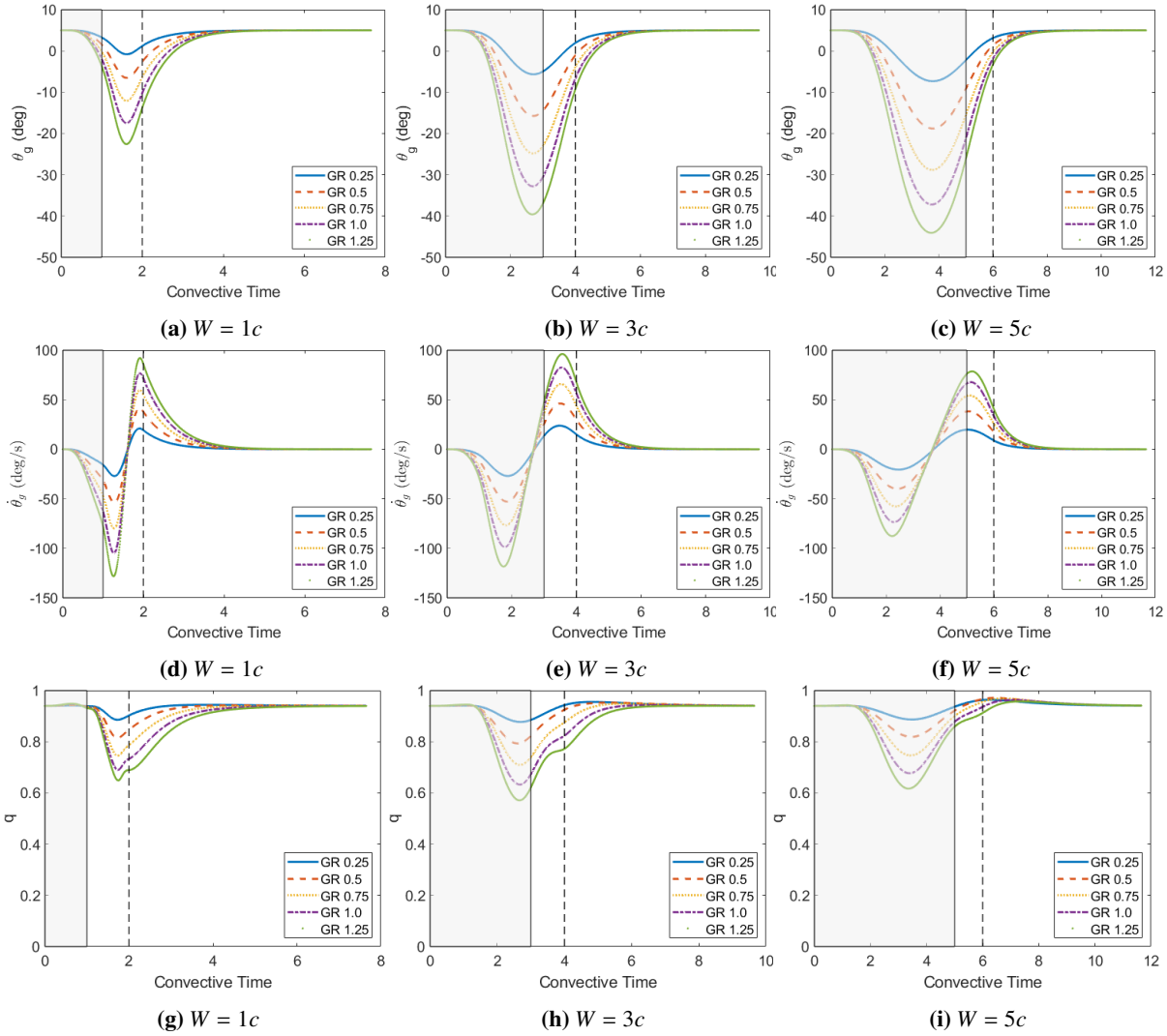

(a) $W = 1c$ **(b)** $W = 3c$ **(c)** $W = 5c$

(d) $W = 1c$ **(e)** $W = 3c$ **(f)** $W = 5c$

(g) $W = 1c$ **(h)** $W = 3c$ **(i)** $W = 5c$

Fig. 5 State vector components of the mGK model during optimal maneuvers in various gust encounters. (a) – (c) $x_1 = \theta_g$**, (d) – (f)** $x_2 = \dot{\theta}_g$**, (g) – (i)** $x_3 = q$**.**

Figure 5 provides insight into state components of the mGK model during the simulated gust encounters, and Fig. 6 shows the effective angle of attack during the simulations. The state variables θ_g and $\dot{\theta}_g$ are related to the wing's pitching motion, and they exhibit a pitch-down, then pitch-up maneuver in all cases. Further, the maneuver magnitude scales with gust ratio for the range of GR = 0.25 to 1.25 with a very little variation. In Fig. 5(g), where the gust width is as narrow as $1c$, the state q does not vary significantly until the leading edge of the wing exits the gust. This delay may be due to the time constant τ_1 in the GK model, since the state components θ_g and $\dot{\theta}_g$ changed during this same period (e.g., see Fig. 5(a) and Fig. 5(d)). In all cases, including the narrow $W = 1c$ gust, the start of maneuvering coincides with changes in the effective angle of attack as shown in Fig. 6(a). Comparison of the $\dot{\theta}_g$ histories to the α_{eff} histories reveals remarkable similarity of the curves — the $\dot{\theta}_g$ profiles appear to be scaled α_{eff} profiles reflected about the horizontal axis. This observation is suggestive that an optimal pitch rate is closely related to the effective angle of attack, which is proportional to the lift output. In Section V.C, this paper examines the relationship between an optimal pitch acceleration and proportional output-feedback control for an mGK gust encounter model.

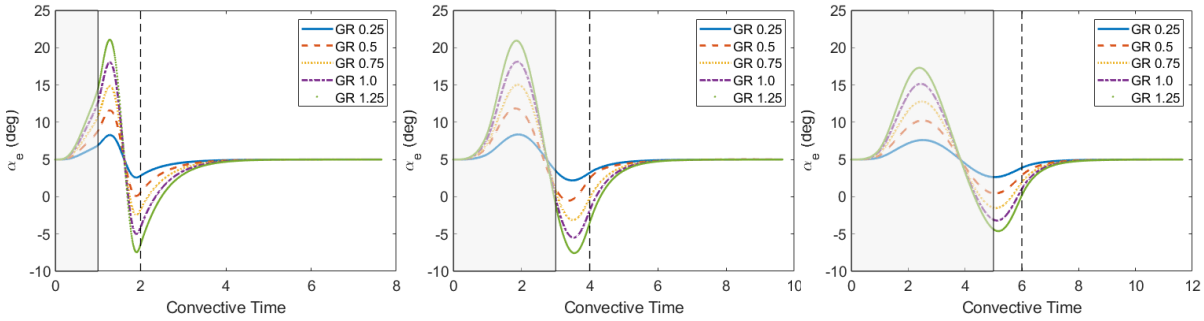

(a) $W = 1c$ **(b)** $W = 3c$ **(c)** $W = 5c$

Fig. 6 Effective angle of attacks during the gust encounters.

B. Optimal Pitch Maneuvers for Various Locations of the Pitch Axis

Apart from the variations in the gust strength and gust width, the dependence of the optimal controller on location of the pitch axis was also studied. The effective angle of attack in (8) captures the effect of the location of the pitch axis with the variable x_C. The location also influences the added-mass force in the output Eq. (10) through the variable a, which is related to x_C by $a = (x_C - b)/b$. Figure 7 shows the pitch acceleration during a transverse gust encounter with GR = 0.5 and $W = 3c$ for three different pitch-axis locations: $x_C = 0, 0.25c$, and $0.5c$ (i.e., $a = -1, -0.5$, and 0). The magnitude of pitch acceleration is largest when pitching at the mid-chord (i.e., $x_C = 0.5c$) and smallest at the leading edge (i.e., $x_C = 0c$). In addition, there is a phase difference between the control signals. Pitching at the leading edge (i.e., $x_C = 0c$) lags the signal for pitching about the other two locations. This behavior may be attributed to the appearance of the control input in the added-mass term in Eq. (10). Note that pitching about the mid-chord (i.e., $x_C = 0.5c$) yields no added-mass contribution to the output. The direct feed-through contribution of the control u to the output increases as the pitch axis moves away from the mid-chord. These observations suggest that the pitch axis plays an important role in influencing an optimal control signal for pitch acceleration.

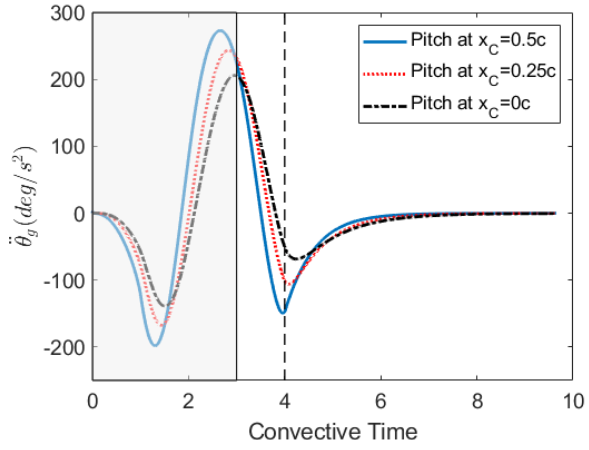

Fig. 7 Optimal pitch acceleration during a lift-regulation maneuver for different pitch axis locations.

C. Comparison to Proportional Output-Feedback Control

Researchers have worked on the design of pitch maneuvers to regulate the lift response in a transverse gust encounter based on GK models and other lift models [6, 8, 24]. Sedky et al. [6] designed a proportional state-feedback controller based on a modified GK model with a Kalman filter to estimate the state vector. Their subsequent work [8] used only proportional output-feedback of the lift signal to pitch a flat plate in a transverse gust encounter modeled using a DVM. In [8], the proportional output-feedback controller effectively regulates lift, which motivates a comparison to an optimal solution. This section considers the comparison of proportional output-feedback control to optimal-control results

derived in this paper. The proportional output feedback controller is:

$$
\begin{aligned}
u_{\text{out}} &= -K\left(C_L - C_{L,\text{ref}}\right) \\
&= -K\left(m_1\left(\alpha_{\text{eff}}\left(\theta_g, \dot{\theta}_g\right)\right) q + m_2\left(\alpha_{\text{eff}}\left(\theta_g, \dot{\theta}_g\right)\right)(1-q) + \frac{\pi b}{\overline{V}}\left(\dot{\theta}_g - \frac{ab}{\overline{V}}\ddot{\theta}_g\right) - C_{L,\text{ref}}\right),
\end{aligned}
\tag{28}
$$

where K is a constant feedback gain that must be selected. This section tests a sequence of different K values for a gust encounter with GR = 0.5 and $W = 3c$.

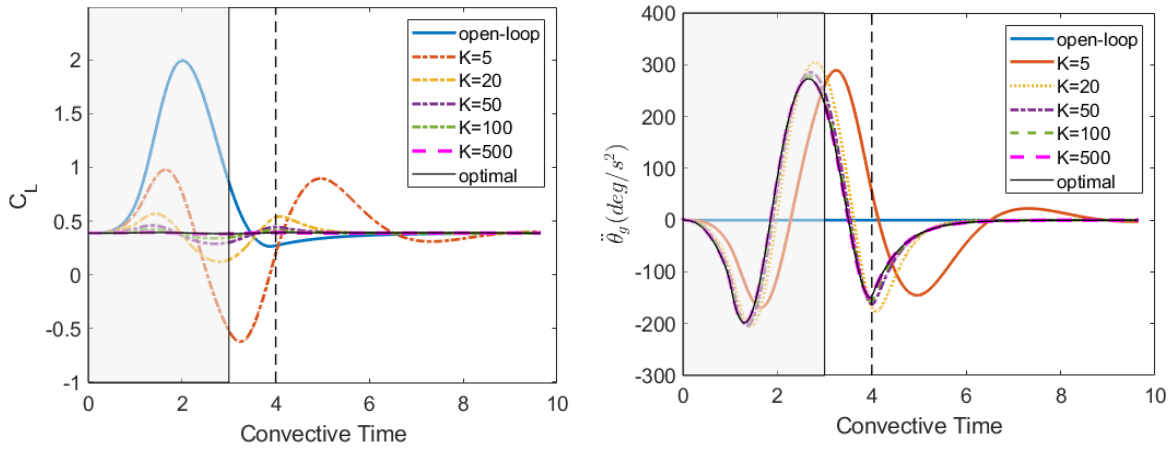

(a) Lift coefficients in the gust encounter

(b) Control profile

Fig. 8 Proportional output-feedback control converging to an optimal control solution.

Figure 8(a) shows the lift coefficient in the gust encounter with the proportional output-feedback controller for different values of feedback gain. When the gain K is small, the lift regulation is poor but with increasing K value, the performance significantly improves. Figure 8(b) shows the corresponding control signals. Note that proportional output-feedback control signal converges to the optimal control signal for $K \geq 500$. The simulation results indicate that the proportional output-feedback controller is optimal for a sufficiently large K. This numerical observation suggests that open-loop optimal control signals can be generated for the mGK model of this paper without optimal control calculations; only simulation of the mGK model with the control choice in Eq. (28) is needed. This finding may perhaps extend to other similarly modified Goman-Khrabrov models, such as the model of Nasipur et al. [21], however further investigation is needed. It is important to note that the consideration of proportional output-feedback control as optimal for large gains, as suggested numerically here, should be limited to the generation of open-loop trajectories. Real data of lift force in experiments and high-fidelity numerical simulations contain noise that would be amplified in the control signal by the feedback gain, leading to poor lift regulation.

VI. Conclusion

This paper applies a gradient-based algorithm from optimal control theory for calculating an optimal pitch maneuver to regulate lift during a transverse gust encounter simulated using a modified Goman-Khrabrov (mGK) model and a sine-squared gust. The gradient-based method searches for a locally optimal control solution. The simulation results show very good performance in lift regulation for gust strengths in the range of GR = 0.25 to 1.25 and gust widths in the range of $W = 1c$ to $5c$. The results are consistent with pitch-down, then pitch-up maneuvers that scale in magnitude for increasing gust ratio. Various control profile changes are present for narrow gusts with $W = 1c$. The changes in the pitch acceleration of different pitch-axis locations are simulated, and the results show pitching at the mid-chord requires greater pitch acceleration during maneuvers. Simulation results indicates that a proportional output-feedback controller can generate optimal control solutions for an mGK model for sufficiently large control gain.

In the ongoing work, the authors are studying the application of the optimal control signal for the mGK model in CFD simulation to examine the performance and consider the physical mechanisms of lift regulation in gust encounters.

Appendix

This section presents derivatives necessary for implementation of Alg. 1 to solve the lift regulation problem of Section IV.B using the mGK gust encounter model of Section III.C.

The 3×3 Jacobian matrix needed for integration of the co-state dynamics

$$\frac{\partial \mathbf{f}}{\partial \mathbf{x}} = \begin{bmatrix} 0 & 1 & 0 \\ 0 & 0 & 0 \\ \frac{1}{\tau_1}\frac{\partial q_0}{\partial \alpha}\left(\frac{\partial \alpha_{\text{eff}}}{\partial x_1} - \tau_2 \frac{\partial \dot{\alpha}_{\text{eff}}}{\partial x_1}\right) & \frac{1}{\tau_1}\frac{\partial q_0}{\partial \alpha}\left(\frac{\partial \alpha_{\text{eff}}}{\partial x_2} - \tau_2 \frac{\partial \dot{\alpha}_{\text{eff}}}{\partial x_2}\right) & -\frac{1}{\tau_1} \end{bmatrix}, \tag{29}$$

where

$$\begin{aligned}
\frac{\partial \alpha_{\text{eff}}}{\partial x_1} &= \frac{-1}{\pi \overline{V}} \int_0^\pi \left(\dot{s} \cos x_1 + u_z \sin x_1\right)\left(\cos\theta_0 - 1\right) d\theta_0 \\
\frac{\partial \dot{\alpha}_{\text{eff}}}{\partial x_1} &= \frac{-1}{\pi \overline{V}} \int_0^\pi \left(-\dot{s} \sin x_1 + \dot{u}_z \sin x_1 + u_z x_2 \cos x_1\right)\left(\cos\theta_0 - 1\right) d\theta_0 \\
\frac{\partial \alpha_{\text{eff}}}{\partial x_2} &= \frac{-1}{\pi \overline{V}} \int_0^\pi \left(b\left(1 - \cos\theta_0\right) - x_C\right)\left(\cos\theta_0 - 1\right) d\theta_0 = \frac{3b - 2x_C}{2\overline{V}} \\
\frac{\partial \dot{\alpha}_{\text{eff}}}{\partial x_2} &= \frac{-1}{\pi \overline{V}} \int_0^\pi \left(\dot{s} \cos x_1 + u_z \sin x_1\right)\left(\cos\theta_0 - 1\right) d\theta_0 .
\end{aligned}$$

The 3×1 control Jacobian matrix for the mGK model is

$$\frac{\partial \mathbf{f}}{\partial u} = \begin{bmatrix} 0 \\ 1 \\ -\frac{\tau_2}{\tau_1}\frac{\partial q_0}{\partial \alpha}\frac{\partial \dot{\alpha}_{\text{eff}}}{\partial u} \end{bmatrix}, \tag{30}$$

where

$$\frac{\partial \dot{\alpha}_{\text{eff}}}{\partial u} = \frac{-1}{\pi \overline{V}} \int_0^\pi \left(b\left(1 - \cos\theta_0\right) - x_C\right)\left(\cos\theta_0 - 1\right) d\theta_0 = \frac{3b - 2x_C}{2\overline{V}}$$

The derivative of the Lagrangian function with respect to the state vector is

$$\frac{\partial L}{\partial \mathbf{x}} = \begin{bmatrix} \frac{\partial L}{\partial x_1} & \frac{\partial L}{\partial x_2} & \frac{\partial L}{\partial x_3} \end{bmatrix},$$

which has components,

$$\begin{aligned}
\frac{\partial L}{\partial x_1} &= \left(y - C_{L,\text{ref}}\right)\left(m_1 x_3 + m_2 - m_2 x_3\right)\frac{\partial \alpha_{\text{eff}}}{\partial x_1} \\
\frac{\partial L}{\partial x_2} &= \left(y - C_{L,\text{ref}}\right)\left(\left(m_1 x_3 + m_2 - m_2 x_3\right)\frac{\partial \alpha_{\text{eff}}}{\partial x_2} + \frac{\pi b}{\overline{V}}\right) \\
\frac{\partial L}{\partial x_3} &= \left(y - C_{L,\text{ref}}\right)\left(m_1 \alpha_{\text{eff}} - m_2 \alpha_{\text{eff}}\right).
\end{aligned} \tag{31}$$

The derivative of the Lagrangian function with respect to the control is a scalar, given by

$$\frac{\partial L}{\partial u} = \left(y - C_{L,\text{ref}}\right)\left(-\frac{\pi b^2 a}{\overline{V}^2}\right). \tag{32}$$

Acknowledgments

This work was supported by the National Science Foundation under grant CBET-2003999, monitored by program officer R. Joslin. The authors gratefully acknowledge valuable discussions with G. Sedky, A. Gementzopoulos, A. R. Jones, and T. Singh.

References

[1] Zarovy, S., Costello, M., Mehta, A., Gremillion, G., Miller, D., Ranganathan, B., Humbert, J. S., and Samuel, P., "Experimental study of gust effects on micro air vehicles," *AIAA Atmospheric Flight Mechanics Conference*, 2010, p. 7818.

[2] Moulin, B., and Karpel, M., "Gust loads alleviation using special control surfaces," *Journal of Aircraft*, Vol. 44, No. 1, 2007, pp. 17–25.

[3] Cook, R. G., Palacios, R., and Goulart, P., "Robust gust alleviation and stabilization of very flexible aircraft," *AIAA journal*, Vol. 51, No. 2, 2013, pp. 330–340.

[4] Bhatia, M., Patil, M., Woolsey, C., Stanford, B., and Beran, P., "Stabilization of Flapping-Wing Micro-Air Vehicles in Gust Environments," *Journal of Guidance, Control, and Dynamics*, Vol. 37, No. 2, 2014, pp. 592–607. doi:10.2514/1.59875, URL https://doi.org/10.2514/1.59875.

[5] Oduyela, A., and Slegers, N., "Gust mitigation of micro air vehicles using passive articulated wings," *The Scientific World Journal*, Vol. 2014, 2014.

[6] Sedky, G., Jones, A. R., and Lagor, F. D., "Lift Regulation During Transverse Gust Encounters Using a Modified Goman–Khrabrov Model," *AIAA Journal*, Vol. 0, No. 0, 2020, pp. 1–11. doi:10.2514/1.J059127, URL https://doi.org/10.2514/1.J059127.

[7] Biler, H., Badrya, C., and Jones, A. R., "Experimental and Computational Investigation of Transverse Gust Encounters," *AIAA Journal*, Vol. 57, No. 11, 2019, pp. 1–15. doi:10.2514/1.j057646.

[8] Sedky, G., Lagor, F. D., and Jones, A., "Unsteady aerodynamics of lift regulation during a transverse gust encounter," *Phys. Rev. Fluids*, Vol. 5, 2020, p. 074701. doi:10.1103/PhysRevFluids.5.074701, URL https://link.aps.org/doi/10.1103/PhysRevFluids.5.074701.

[9] Andreu-Angulo, I., Babinsky, H., Biler, H., Sedky, G., and Jones, A. R., "Effect of Transverse Gust Velocity Profiles," *AIAA Journal*, Vol. 58, No. 12, 2020, pp. 5123–5133.

[10] Leishman, G. J., *Principles of helicopter aerodynamics*, Cambridge University Press, 2006.

[11] Xu, X., and Lagor, F. D., "Quasi-Steady Effective Angle of Attack and Its Use in Lift-Equivalent Motion Design," *AIAA Journal*, Vol. 0, No. 0, 0, pp. 1–14. doi:10.2514/1.J059663, URL https://doi.org/10.2514/1.J059663.

[12] Theodorsen, T., and Mutchler, W., "General theory of aerodynamic instability and the mechanism of flutter," 1935.

[13] Wagner, H., "Über die Entstehung des dynamischen Auftriebes von Tragflügeln," *ZAMM-Journal of Applied Mathematics and Mechanics/Zeitschrift für Angewandte Mathematik und Mechanik*, Vol. 5, No. 1, 1925, pp. 17–35.

[14] Küssner, H. G., "Zusammenfassender Bericht über den instationären Auftrieb von Flügeln," *Luftfahrtforschung*, Vol. 13, No. 12, 1936, pp. 410–424.

[15] von Kármán, T., "Airfoil Theory for Non-Uniform Motion," *Journal of the Aeronautical Sciences*, Vol. 5, No. 10, 1938, pp. 379–390. doi:10.2514/8.674.

[16] Goman, M., and Khrabrov, A., "State-space representation of aerodynamic characteristics of an aircraft at high angles of attack," *Journal of Aircraft*, Vol. 31, No. 5, 1994, pp. 1109–1115. doi:10.2514/3.46618, URL https://doi.org/10.2514/3.46618.

[17] Greenblatt, D., Mueller-Vahl, H., Williams, D. R., and Reissner, F., "Goman-Khrabrov Model on a Pitching Airfoil with Flow Control," *8th AIAA Flow Control Conference*, 2016. doi:10.2514/6.2016-4240, URL https://arc.aiaa.org/doi/abs/10.2514/6.2016-4240.

[18] An, X., Grimaud, L., and Williams, D. R., "Feedforward Control of Lift Hysteresis during Periodic and Random Pitching Maneuvers," *Active Flow and Combustion Control 2014*, edited by R. King, Springer International Publishing, Cham, 2015, pp. 55–69.

[19] Williams, D. R., An, X., Iliev, S., King, R., and Reißner, F., "Dynamic hysteresis control of lift on a pitching wing," *Experiments in Fluids*, Vol. 56, No. 5, 2015, p. 112.

[20] Williams, D. R., and King, R., "Alleviating Unsteady Aerodynamic Loads with Closed-Loop Flow Control," *AIAA Journal*, Vol. 56, No. 6, 2018, pp. 2194–2207. doi:10.2514/1.J056817, URL https://doi.org/10.2514/1.J056817.

[21] Narsipur, S., Gopalarathnam, A., and Edwards, J. R., "Low-Order Model for Prediction of Trailing-Edge Separation in Unsteady Flow," *AIAA Journal*, Vol. 57, No. 1, 2019, pp. 191–207. doi:10.2514/1.J057132.

[22] Ramesh, K., Gopalarathnam, A., Granlund, K., Ol, M. V., and Edwards, J. R., "Discrete-Vortex Method with Novel Shedding Criterion for Unsteady Aerofoil Flows with Intermittent Leading-Edge Vortex Shedding," *Journal of Fluid Mechanics*, Vol. 751, 2014, pp. 500–538. doi:10.1017/jfm.2014.297.

[23] Angulo, I. A., and Babinsky, H., *Negating Gust Effects by Actively Pitching a Wing*, AIAA Scitech 2020 Forum. doi: 10.2514/6.2020-1057, URL https://arc.aiaa.org/doi/abs/10.2514/6.2020-1057.

[24] Angulo, I. A., and Babinsky, H., *Unsteady Modelling of Pitching Wings for Gust Mitigation*, AIAA Scitech 2021 Forum. doi:10.2514/6.2021-1999, URL https://arc.aiaa.org/doi/abs/10.2514/6.2021-1999.

[25] Williams, D. R., Reißner, F., Greenblatt, D., Müller-Vahl, H., and Strangfeld, C., "Modeling Lift Hysteresis on Pitching Airfoils with a Modified Goman–Khrabrov Model," *AIAA Journal*, Vol. 55, No. 2, 2017, pp. 403–409. doi:10.2514/1.J054937, URL https://doi.org/10.2514/1.J054937.

[26] Sedky, G., Jones, A. R., and Lagor, F., "Lift modeling and regulation for a finite wing during transverse gust encounters," *AIAA Scitech 2019 Forum*, 2019, p. 1146.

[27] Darwin, C., "Note on hydrodynamics," *Mathematical Proceedings of the Cambridge Philosophical Society*, Vol. 49, Cambridge University Press, 1953, pp. 342–354.

[28] Bryson, A. E., and Ho, Y.-C., *Applied optimal control: optimization, estimation, and control*, Routledge, 1975.